Fluorescence spectroscopy of low-level endogenous β-Adrenergic Receptor expression at the plasma membrane of differentiating human iPSC-derived cardiomyocytes

Philipp Gmach[1,2*], Marc Bathe-Peters[1*], Narasimha Telugu[1], Martin J Lohse[1,2,3], Paolo Annibale[#1,4]

[1]Max Delbrück Center for Molecular Medicine in the Helmholtz Association, Berlin, Germany

[2]Institute of Pharmacology and Toxicology, University of Würzburg, Würzburg, Germany

[3]ISAR Bioscience Institute, 82152 Munich-Planegg, Germany

[4]School of Physics and Astronomy, University of St Andrews, St Andrews, United Kingdom

[#]Correspondence to pa53@st-andrews.ac.uk

* Contributed equally (PG and MBP)

Abstract

The potential of human induced pluripotent stem cells (hiPSCs) to be differentiated into cardiomyocytes (CMs) mimicking the adult CMs functional morphology, marker genes and signaling characteristics has been investigated since over a decade. The evolution of the membrane localization of CM-specific G protein-coupled receptors throughout differentiation has received, however, only limited attention to date. We employ here advanced fluorescent spectroscopy, namely linescan Fluorescence Correlation Spectroscopy (FCS), to observe how the plasma membrane abundance of the β_1- and β_2-adrenergic receptors ($\beta_{1/2}$-ARs), labelled using a bright and photostable fluorescent antagonist, evolves during long-term monolayer culture of hiPSC-derived CMs. We compare it to the kinetic of observed mRNA levels, in wildtype (WT) hiPSCs and in two knock-in CRISPR clones. We conduct these observations against the backdrop of our recent report that β_2-ARs, as opposed to β_1-ARs, specifically segregate to the T-Tubular system of adult CMs.

Introduction

Human induced pluripotent stem cells (hiPSCs) can be differentiated into cardiomyocytes (CMs) that are functionally comparable to embryonic stem (ES) cell–derived CMs and/or mimicking the functional morphology of adult cardiomyocytes. Although fully differentiated hiPSCs do not yet achieve a phenotype entirely reminiscent of that of adult CMs - an area of active and intense research [1] - the possibility of driving in a controlled way these cells from a pluripotent towards a more mature phenotype offers several important unique

opportunities. First and foremost, undifferentiated hiPSCs are amenable to genetic editing, which allows them to incorporate knockouts of selected genes or addition of functional tags, such as fluorophores, that will then be carried forward to the CM phenotype.

Secondly, expression of key genes changes over time and this can be followed in detail, providing an insight into how key structures of the CM phenotype originate, and how specific signaling pathways and their associated molecular mechanisms develop. In this respect, several works have explored since almost 20 years the evolution of the transcriptome of hiPSCs as they directionally differentiate towards CMs. The majority of CM-specific genes seem to be upregulated after day 14 [2]. More recently, single cell sequencing has allowed to shed light also on cell-to-cell expression variability for selected genes [3] [4].

An important feature of adult CMs is the ability to increase or reduce both strength and frequency of their contractions in response to external stimuli, two processes that go under the name of inotropic and chronotropic responses, respectively. The β-adrenergic system, embodied by the β_1- and β_2-adrenergic receptors (β-ARs, expressed from the *ADRB1* and *ADRB2* genes respectively), represents the typical pathway mediating catecholamine-driven inotropic and chronotropic responses, and is a crucial therapeutic target in the context of heart failure, mostly thanks to the discovery of the beneficial action of negative inotropes/chronotopes such as β-blockers. In the adult heart, β_1 and β_2 are both expressed, with a ratio of β_1/β_2-ARs of around 70%–80%/30%–20% in human ventricles [5-7].

The evolution of endogenous β-AR expression over maturation time in hiPSCs directionally differentiated towards CMs has thus been explored in several recent works. Wu et al. observed mRNA levels and effects on contractility of β-AR expression in differentiating hiPSC, in a model of dilated cardiomyopathy [5]. Jung et al. studied adrenoreceptor mRNA levels within the context of functional remodelling [8], while Hasan et al. monitored how receptor-specific cAMP signaling evolves throughout hiPSC differentiation towards CMs [9]. Kondrashov et al. studied the temporal dynamics of β_2-AR expression in CRISPRed hiPSC [10]. An earlier work by Yan et al. studied the effect of adrenergic signalling on regulating cardiac differentiation of mouse embryonic stem cells and monitored *ADRB1* and *ADRB2* expression as a function of time [11].

These works interestingly report a predominant *ADRB2* expression with respect to *ADRB1*, resulting in a higher second messenger production upon selective β_2-AR stimulation, that then decays during differentiation. This results in a β_2-AR dominated functional response (contractility) which is then caught-up by the β_1-AR at day 60. These results point to the interesting and persistent gene expression dynamics affecting the relative weight of these two key adrenoreceptors. However, transcriptomic analyses and functional downstream readouts, even if conducted at the single cell level, fail to provide information about what occurs in terms of 1. protein expression and 2. receptor localization. We believe this is an important aspect to consider, in the light of our recent

observation of the peculiar differential localization of the β_1- and β_2-ARs on the membranes of adult cardiomyocytes [12]. We could show that the β_2-AR partitions to the T-tubular network of the cardiomyocyte and does not appear to diffuse upon the basolateral ('crest') surface plasma membrane of the cell, thus explaining the compartmentalized cAMP signal observed earlier in this cell-type [13].

Key to our observation was the use of a high-sensitivity fluorescence spectroscopy method, namely linescan-FCS [14], that allowed us appreciating minute amounts of endogenous receptors diffusing on the membranes using a fluorescent antagonist. In that context we could also observe, not only significant CM to CM variability of receptor expression (i.e. β_1-AR is visible only in 60% of the cells considered), but also the fact that, in CM-like cells such as H9c2 and CM-differentiated hiPSC, β_2-ARs were clearly seen diffusing on the basolateral membrane.

We thus reasoned that it is now timely to investigate how the plasma membrane concentration of the β_1- and β_2-adrenergic receptors evolves during long-term monolayer culture of hiPSC-CM, whilst comparing it to the measured mRNA levels. Moreover, considering that one of the key advantages of hiPSCs is their ability of being gene-edited in their pluripotent, non-differentiated state, we extended our analysis also to two hiPSC clones carrying a heterozygous and a homozygous CRISPR-mediated knock-in of a fluorescent tag at the N-terminus of the *ADRB2*. This should further allow to corroborate the missing link between protein localization and mRNA levels.

We could observe that in wildtype (WT) hiPSCs, there is a discrepancy between β_2-AR appearance at the surface plasma membrane during early maturation stages (day25) with respect to the measured mRNA levels, and a significant cell-to-cell heterogeneity in receptor abundance at the plasma membrane. At later maturation stages (day60) mRNA levels correlated with membrane appearance of β_2-AR in WT hiPSC-CM as well as in CRISPRed hiPSC-CM clones, indicating that the addition of a tag at the N-terminus of ADRB2/β_2-AR still allowed for correct receptor transcription, expression and localization at and after day 60.

These observations open fascinating questions on the mechanisms that control and time receptors appearance and distribution at the plasma membrane, with potential implication towards better understanding of a signaling cascade at the core of heart pathophysiology and failure.

Results

We first set to establish a CM-differentiation assay for hiPSCs (See Methods), identifying timepoints (0, 25, 60 and 100 days) after onset of differentiation for our investigation (**Supplementary Figure 1**). The hiPSCs morphology was investigated by transmitted light microscopy, as reported in **Figure 1a and Supplementary Figure 1a**.

We worked with three hiPS cell lines - WT hiPSCs, and two clonal lines arising respectively from a heterozygous (66-35) and homozygous knock-in (16-31) of the monomeric Enhanced Green Fluorescent Protein (mEGFP) at the N-terminus of the endogenous *ADRB2* gene locus. Clones 16-31 and 66-35, created using CRISPR/Cas9 editing in combination with a novel hybrid, partially single-stranded DNA-based HDR donor cocktail, and details of the knock-in procedure as well as the clones' characterization are described in **Supplementary Figure 2** and the **Methods**.

Figure 1a further displays fluorescence excitation of the cells at 488 nm, indicating a substantial amount of autofluorescence[15] [16], that increases as cells differentiate towards a mature CM phenotype. Interestingly, the level of green signal is comparable between the WT cells and the two mEGFP knock-in clones, suggesting that the very low-level expression of the tagged β_2-AR has to compete with autofluorescence, and that alternative tagging strategies shall be considered [17, 18]. In the following, we therefore employed the fluorescent antagonist which we successfully used in our recent spectroscopic imaging of adrenergic receptors in adult murine cardiomyocytes (JE1319 [12]), while still exploiting the information arising from the two knock-in clones.

Figure 1b displays the fully differentiated hiPSC-CM phenotype at day ~100, employing α-actinin and troponin T immunofluorescence to highlight the presence of sarcomeric structures and thus the success of differentiation. This shall be compared to the lower immunofluorescence signal observed in the few non-CM cells present in the culture (dashed lines in the DIC and Merge overlay of Fig. 1B). Morphologically, there are no detectable differences between the WT cells and clones 16-31 and 66-35.

When subjected to selective adrenergic stimulation (for either β_1-AR using ICI-118551 or β_2-AR using CGP-20712A) (**Figure 1c**), the day ~100 hiPSC-CM displayed a chronotropic response, as measured by their beating rate, comparable between the WT cells and the homozygous clone 16-31. In particular, the selective β_2-AR stimulation displayed an increase in beating rate almost identical between the WT and the knock-in, suggesting that N-terminal tagging of the β_2-AR is neither affecting its proper expression nor its function. These results also confirm that, almost undetectable levels of expressed receptor can contribute to the normal response of the cell to external stimuli [12].

Having established and characterized our three hiPSC-CM cell lines, we now set to explore in detail the kinetic of β_2-ARs expression as a function of the maturation time. In order to do so, we first performed quantitative mRNA measurements using qRT-PCR (**see Methods**). Here, the presence of a tag in the two knock-in clones further allows to measure the expression levels of individual alleles, as well as to compare transcript levels from a tagged variant of the β_2-AR to its WT expression. The results of this experiment are displayed in **Figure 2:** here, we compare absolute mRNA levels (**Figure 2a**) extracted from cultures of WT hiPSC and our two clones. Two sets of qPCR primers, as detailed in the methods, one complementary to the mEGFP sequence (green bars) and the other complementary to the *ADRB2* nucleotide sequence (black bars) were used, thus allowing

to compare expression level of the endogenous background with respect to the tagged allele(s) (**see Methods**).

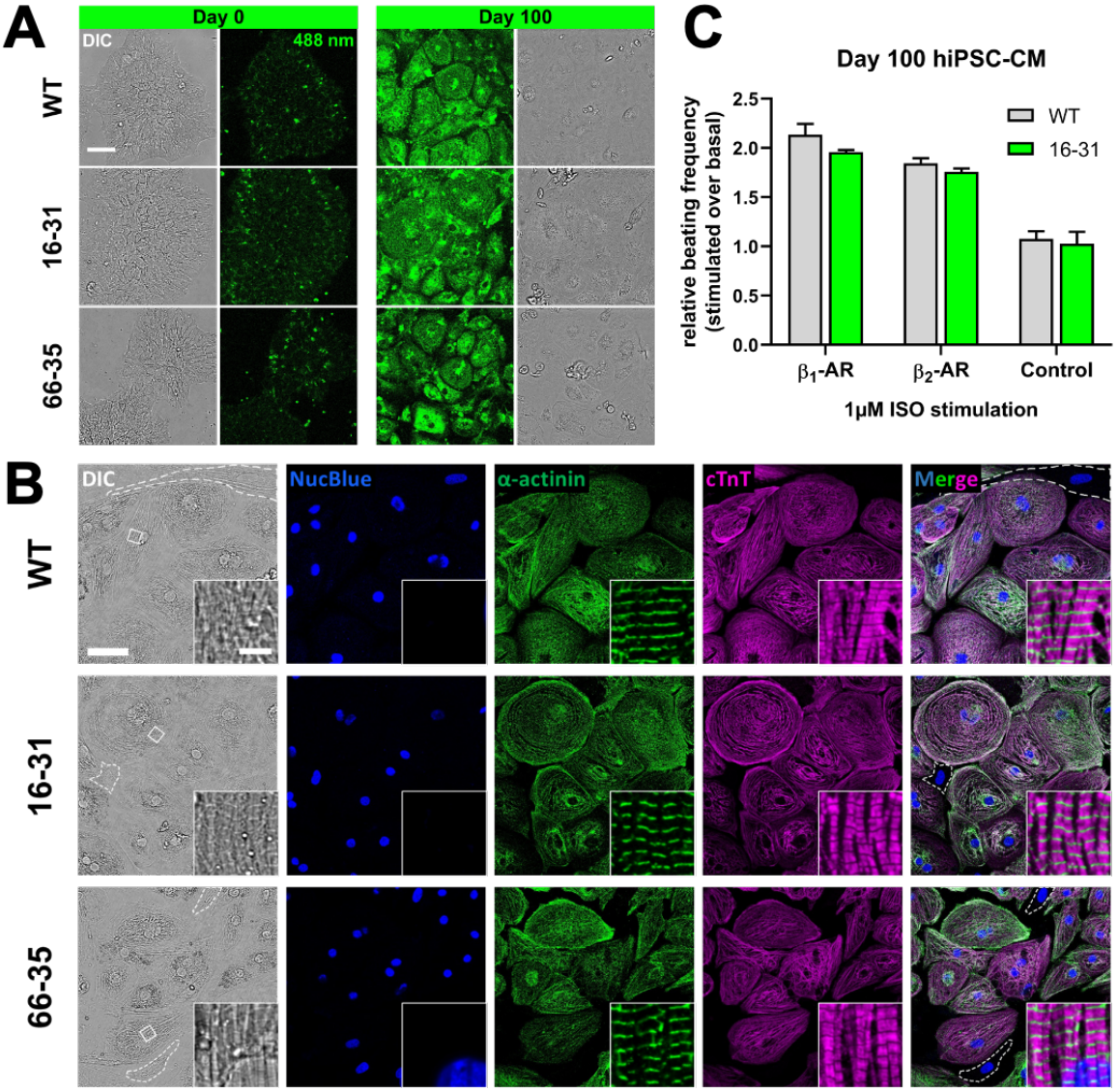

Figure 1 Maturation state of hiPSC-CMs. (A) Comparison of undifferentiated (day 0) and differentiated (day 100) WT hiPSC-CM and mEGFP-ADRB2 CRISPRed clones 16-31 and 66-35. Fluorescence images represent autofluorescence in the green spectral range at 488 nm. Shown are representative images of 2 replicates with imaging of ≥4 points-of-view. Contrast settings are identical. Scale bar is 50 μm. (B) Immunofluorescence staining of day 100 WT hiPSC-CM and clones 16-31 and 66-35 for typical cardiomyocyte markers α-actinin and cardiac troponin T (cTnT). Nuclei were stained with NucBlue. Insets show magnifications of regions marked with white rectangles in DIC. Dashed lines in DIC and merge indicate cells lacking a cardiac phenotype, most likely fibroblasts. Representative images of 3 replicates with imaging of ≥3 points-of-view are shown. Scale bar is 50 μm and in magnification 5 μm. (C) Functionality recording of WT hiPSC-CMs and clone 16-31 after 100 days of differentiation. Shown is the increase in beating frequency normalized to basal frequency upon stimulation with 1 μM

isoproterenol (ISO) of β_1-ARs and β_2-ARs. The frequency remains unchanged upon stimulation after blocking the receptors with 10 μM propranolol (Control). Graph represents the mean ±SEM of ≥3 independent experiments.

Upon normalization to *GAPDH* and the day 0 expression levels of the homozygous clone 16-31, **Figure 2b** allows to fully appreciate the temporal evolution of ADRB2 transcripts amount along the differentiation pathway. In accordance to what was observed in previous reports [5], *ADRB2* mRNA transcripts appear to be substantially upregulated already after day 25 from the onset of differentiation, with modest increases along the further timepoints. As expected, clone 16-31 displays comparable expression levels of mRNA containing the mEGFP sequence and of mRNA containing the ADRB2 coding sequence, indicative that both alleles carry the knock-in. Instead, clone 66-35 displays roughly half mEGFP mRNA than *ADRB2* mRNA, indicative for both a monoallelic knock-in as well as of a roughly equal level of expression of both alleles throughout the differentiation. In the light of these observations, we ascribe here the lower overall ADRB2 mRNA levels observed in both clone 16-31 and clone 66-35 to clonal variability.

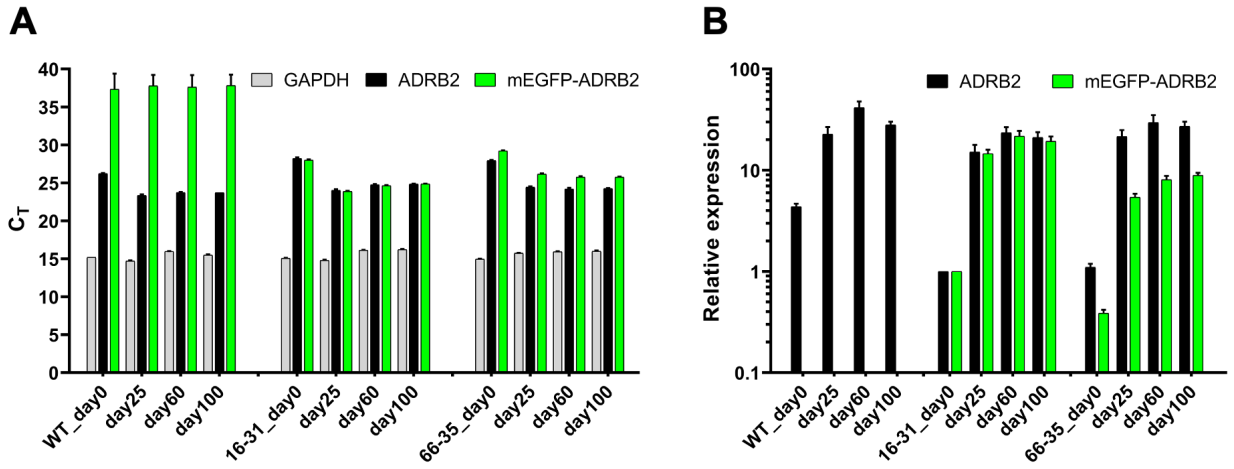

Figure 2 Indication of endogenous ADRB2 and mEGFP-*ADRB2* mRNA expression during hiPSC-CM culture maturation. (A) Absolute cycle threshold (c_T) values for GAPDH, ADRB2 and mEGFP-ADRB2 are shown. (B) Relative expression of data shown in A) normalized to GAPDH and calibrated to day 0 of clone 16-31. Data are mean ±SD of (3-6 replicates of) 2 independent experiments.

The next question is now if and how mRNA expression levels of the *ADRB2* over time are mirrored by the β_2-AR expression levels at the plasma membrane. In order to measure the latter, we resort to the approach we already successfully used to monitor β-AR expression in adult CMs, based on linescan-FCS to monitor minute amounts of diffusing receptors tagged with our fluorescently labeled antagonist. Briefly, the excitation volume of the confocal microscope is scanned rapidly (< 1 ms) along a line, positioned along the basolateral membrane of the cell. Fluctuations due to the diffusion of the tagged receptors are extracted by a mathematical analysis known as autocorrelation, to yield a curve termed autocorrelation function (ACF), that contains information both on the diffusivity

and concentration of the tagged receptors. This function can be then displayed in a color code, and average ACF from several cells pooled in a heatmap image, that allows direct comparison between and across clones and timepoints. In general, the qualitative observation of an ACF, with decaying amplitude (from red – high correlation to blue – no correlation) indicates the presence and diffusion of labeled receptors. For this reason, the method can be used in a powerful way to estimate the presence of the β_1-AR and β_2-AR at the basolateral membrane in our hiPSC clones, and measure their evolution over time. The result of this analysis is displayed for the WT hiPSC-CM in **Figure 3,** comparing β_1-AR and β_2-AR expression over time. Most of the undifferentiated (day 0) cells display low to negligible level of β_1-AR and β_2-AR expression, with the exception of one cell where β_2-AR was selectively labeled. Along these lines the day 25 cells investigated still displayed a substantial cell-to-cell heterogeneity in plasma membrane expression, with a significant amount of cells still displaying no-trace of either β_1-AR (~90%) or β_2-AR (~75%) at the cell membrane. This is a striking departure from the mRNA data reported in **Figure 2,** as the single cell plasma membrane receptor abundance data paint a significantly more complex, and heterogeneous, picture than the bulk mRNA levels. Both receptors become visible at the plasma membrane in most cells at 60 days from the onset of differentiation, and no qualitative difference is observed between day 60 and day 100. These results open an interesting paradox, since this would imply that at 25 days post differentiation the cell has substantial amounts of *ADRB2* mRNA, but still no comparable levels of β_2-AR expressed at the plasma membrane, pointing to either a limitation on translation of the receptor mRNA or of its correct targeting, as cells progress at different paces through the differentiation pathway.

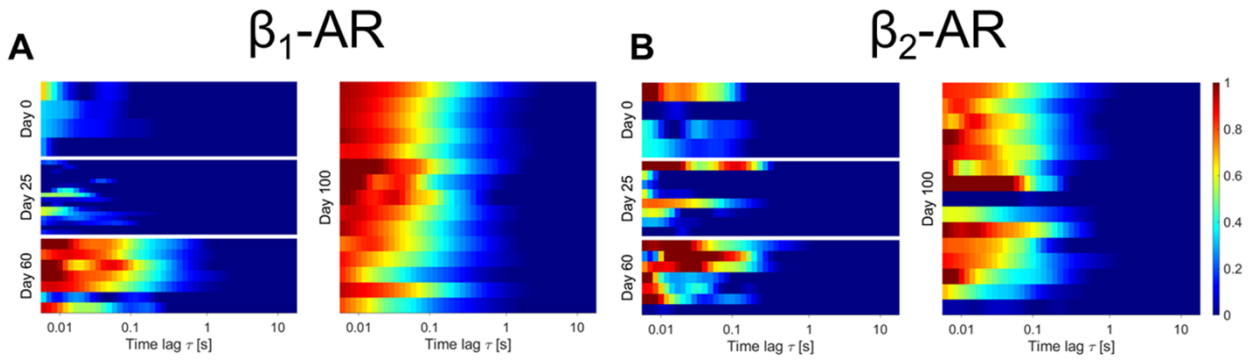

Figure 3 Linescan FCS evaluation of β_1-ARs (A) and β_2-ARs (B) in WT hiPSC-CMs at day 0, 25, 60 and 100 of maturation. For each day a minimum of at least 4 scans of different hiPSC-CMs is evaluated. Colorscale indicates the amplitude of normalized autocorrelation (ACF) curves. Normalization was to each G(0) or highest peak of the curve. Each row represents the average correlation arising from the scan at the surface of one cell.

We further extracted the diffusion constants (found in **Supplemental Figure 3A**) and mean values range from 0.25 – 0.45 $\frac{\mu m^2}{s}$. **Supplemental Figure 3B** gives an indication of the observed receptor concentrations, with mean values ranging from 3 – 12 particles in the effective detection volume of the confocal microscope. In our hands, β_2-AR expression appears higher than β_1-AR both at day 60 and day 100.

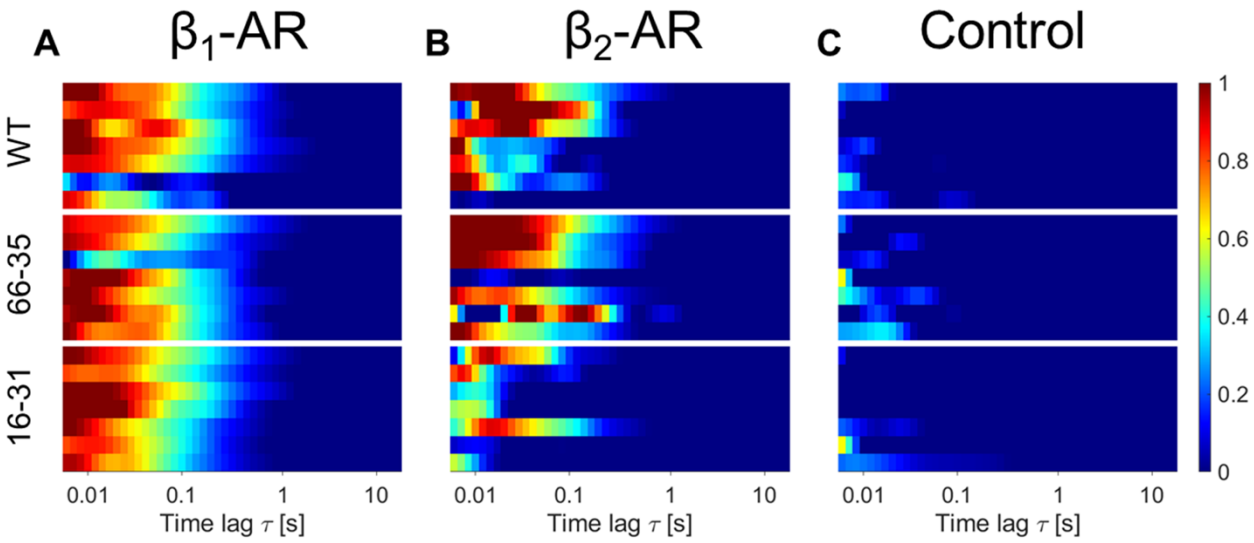

Figure 4 Comparison of β_1-ARs (A) and β_2-ARs (B) membrane expression in hiPSC-CMs at day 60 of maturation. (C) Shows the acquired linescan FCS data of hiPSC-CMs at day 60 of maturation pre-treated with 100 μM propranolol (Control). Each subpanel represents wildtype (WT) hiPSC-CMs (top), clone 66-35 (middle) and clone 16-31 (bottom) and evaluates 4 cells. Colorscale indicates the amplitude of normalized autocorrelation curves. Normalized was to each G(0) or highest peak of the curve. Each bar represents the scan at the surface of one cell. Both receptor subtypes show a diffusional fingerprint at the surface plasma membrane of the WT cells and clones at day 60. Control cells indicate no detected diffusing receptors (blue).

We finally asked whether the knock-in of an N-terminal tag, that did not seem to affect mRNA levels, ended up influencing proper receptor localization at the plasma membrane. The construct corresponding to our knock-in modification of the *ADRB2,* appears to be well expressed and clearly localized to the plasma membrane when transfected, as a plasmid, into H9c2 cells **Supplemental Figure 4**. **Figure 4** displays, for day 60 (when full expression of the receptor on the plasma membrane is observed) that membrane expression levels are comparable between WT hiPSC-CM and the two knock-in clones, with the possible exception of β_2-AR membrane expression on the homozygous clone (16-31). Reassuringly, no membrane signal compatible with receptor diffusion was observed in the control, namely cells treated with the inverse agonist propranolol before being exposed to the fluorescent ligand, did not display any ACF (**Figure 4c**).

The data from β_2-AR on day 60 of clone 16-31, display visible receptor presence at the membrane and dynamics, at least for three of the cells, whereas the other four cells do not yield a signal compatible with receptor diffusing at the membrane. Taken together with the observation of the sizable β_2-AR-mediated increase in contractility (**Figure 1c**), we believe that clone 16-31 is properly expressing the tagged β_2-ARs to the plasma membrane, albeit displaying higher cell to cell variability.

Discussion

Our work has quantitatively explored the membrane expression level of the β_1-AR and β_2-AR in differentiating hiPSCs at four time points, i.e. in the undifferentiated pluripotent state, and then 25, 60 and 100 days after directed differentiation towards a CM state. Our work was conducted in parallel on WT hiPSCs, together with two CRISPR/Cas9 knock-in clones, incorporating respectively a homozygous and heterozygous N-terminal tag (mEGFP) at the β_2-AR, allowing to monitor the effect of a tag on the transcription of the *ADRB2* gene, as well as on the expression and localization of the β_2-AR.

Membrane protein abundance, measured by linescan-FCS, a sensitive fluorescence spectroscopy approach, was then compared to mRNA levels obtained from qPCR. It shall be noted that antibodies raised against GPCRs have well documented shortcomings, and even when using anti-EGFP antibodies against the N-terminal tag in clones 16-31 and 66-35, we failed to detect receptor expression in Western blots (data not shown), reaffirming the necessity of a high-sensitivity method such as our linescan-FCS.

The approach we implemented allowed us to observe a significant discrepancy between mRNA levels of the β_2-AR expression at the plasma membrane 25 days after differentiation, which raises interesting questions concerning translational regulation mechanisms for *ADRB1/2* in differentiating hiPSC-CMs. Our work fills a gap in existing literature, which either addressed only mRNA levels, or functional readouts after day 30 of differentiation in hiPSCs. So far, only one work in mouse ES cells measured protein expression levels as a function of differentiation [11]. The relationship between mRNA levels and protein levels in mammalian cells is complex, and although a general correlation is expected, making transcriptional control the dominant mechanism regulating also protein abundance, there are several exceptions to this rule, as reviewed by Liu et al [19]. In differentiating cells, the situation is even more complex, and translational control has been indicated to play a major role, especially in the early stages of differentiation [20]. We shall note here that our method allows only to monitor receptor expression levels at the basolateral membrane, since we use a ligand non permeable to the plasma membrane [12], and we thus cannot rule out that the β_2-AR is still translated, but does not localize to the plasma membrane. It could be that accessory proteins responsible for its trafficking or posttranslational modifications are not yet present in the differentiating cell at day 0 and day 25 [21]. It shall be further noted that the fully CM-differentiated hiPSCs, even at day ~100, do not display a complete T-Tubular network, leaving open the question if the β_2-AR, that in this work we observed on the basolateral membrane, would eventually segregate in these compartments [12]. Our observation of higher relative β_2-AR expression levels in hiPSC-CMs appears to be in line with what was previously reported in at least three works [5, 8, 9].

We shall also note here that our choice of mEGFP as an N-terminal tag for live cell imaging of the β_2-AR, while well established in overexpression systems, faced significant challenges due to the high autofluorescence background of differentiated hiPSC-CMs, as

displayed in **Figure 1a**. Nevertheless, the use of the tag was instrumental in confirming that the effect of the addition of a 700 bp sequence to the ADRB2 gene, resulting in a ~25 kDa tag on the final protein, did not perturb its transcription, its translation nor its final plasma membrane localization.

Overall, we can show here that linescan-FCS can be successfully used to monitor endogenous low level membrane receptor expression of GPCRs in differentiating hiPSC-CM lines, as recently demonstrated for single point FCS by Goulding et al. in HEK293 cells [17]. This substantially increases the possibilities of current methods available for the assessment of gene expression throughout hiPSC differentiation: not only we add to quantitative mRNA measurements also the dimension of actual protein expression levels, but furthermore we show how to measure it in a spatially resolved way within a single cell.

Materials and methods

Differentiation and culture of hiPSC-CM

hiPSCs (line BIHi005-A) were received from and validated by the stem cell core facility of the Max Delbrück Center for Molecular Medicine. While pluripotent cultures were grown at 37 °C with 5% CO2 and 5% O2, differentiated cultures were maintained at 5% CO2 and atmospheric (21%) O_2. Monolayers of hiPSC were differentiated into CM-hiPSC by modulating Wnt signaling following a small molecule-based cardiac differentiation strategy and enriched for cardiac myocytes by metabolic lactate selection as previously described [12, 22]. In short, hiPSC were cultured in essential 8 basal medium (E8 medium) (Gibco) on Geltrex- (Gibco) coated plates 4 days prior to cardiac induction. As soon as they reached 80-90% confluency, mesodermal differentiation was induced on day 0 for 24 h by changing the medium to cardiac priming medium composed of RPMI 1640 (Gibco), 1x B27 supplement without insulin (Gibco) and 6 µM CHIR99021 (Sellek Chem). On the following day basal differentiation medium (cardiac priming medium without CHIR99021) was added on top of the old cardiac priming medium. Cardiogenesis was induced on day 3 by changing the medium to basal differentiation medium supplemented with 5 µM of the Wnt inhibitor IWR-1 (Sellek Chem). On day 5, without removing the old medium, basal differentiation medium was added to let cells grow for 2 more days. From day 7 onwards, cells were cultured in maintenance medium (RPMI 1640, B27 with insulin (Gibco)) which was exchanged every 3 days. On day 9, cells were selected for cardiomyocytes over 4 days in RPMI 1640 without glucose (Gibco) supplemented with CDM3 supplement (Sigma Aldrich) and 5 mM sodium DL-lactate (Sigma Aldrich). The beating CM-hiPSCs were then cultured in maintenance medium which was exchanged every 3-5 days. Three days prior to imaging CM-hiPSC were detached as single cells and seeded in Geltrex-coated µ-slides (Ibidi). Until the day of experiment CM-hiPSC were cultured in maintenance medium with 3 µM CHIR99021 and 1x RevitaCell supplement (Life Technologies).

Culture of H9c2 cells

H9c2 (ATCC; CRL-1446) cells were maintained in Dulbecco's modified Eagle's medium (PAN-Biotech) supplemented with 10% (vol/vol) fetal bovine serum (FBS) (Sigma-Aldrich), 2 mM L-glutamine (PAN-Biotech), penicillin (100 U/mL; Gibco), and streptomycin (100 µg/mL; Gibco) at 37 °C and 5% CO2. For passaging, cells were detached using trypsin 0.05%/(ethylenedinitrilo)tetraacetic acid (EDTA) 0.02% in phosphate buffered saline (PBS) (PAN-Biotech). The cells were transfected using Lipofectamine (Life Technologies) according to the manufacturer's specification.

Oligonucleotides

Name	Sequence from 5' to 3'	Description
crRNA-103forw	CCTGCCAGACTGCGCGCCAT	crRNA used in combination with generic tracrRNA to build the gRNA for Cas9 targeting to *ADRB2* locus. Binds over start codon for knock-in of mEGFP
Donor plasmid for knock-in of mEGFP	AAGCTTAACGGGCAGAACGCACTGCGAAGCGGCTTCTTCAGAGCAC GGGCTGGAACTGGCAGGCACCGCGAGCCCCTAGCACCCGACAAGC TGAGTGTGCAGGACGAGTCCCCACCACACCCACACCACAGCCGCTG AATGAGGCTTCCAGGCGTCCGCTCGCGGCCCGCAGAGCCCCGCCG TGGGTCCGCCCGCTGAGGCGCCCCCAGCCAGTGCGCTCACCTGCC AGACTGCGCGCCATGGTGAGCAAGGGCGAGGAGCTGTTCACCGGG GTGGTGCCCATCCTGGTCGAGCTGGACGGCGACGTAAACGGCCACA AGTTCAGCGTGTCCGGCGAGGGCGAGGGCGATGCCACCTACGGCA AGCTGACCCTGAAGTTCATCTGCACCACCGGCAAGCTGCCCGTGCC CTGGCCCACCCTCGTGACCACCCTGACCTACGGCGTGCAGTGCTTC AGCCGCTACCCCGACCACATGAAGCAGCACGACTTCTTCAAGTCCG CCATGCCCGAAGGCTACGTCCAGGAGCGCACCATCTTCTTCAAGGA CGACGGCAACTACAAGACCCGCGCCGAGGTGAAGTTCGAGGGCGA CACCCTGGTGAACCGCATCGAGCTGAAGGGCATCGACTTCAAGGAG GACGGCAACATCCTGGGGCACAAGCTGGAGTACAACTACAACAGCC ACAACGTCTATATCATGGCCGACAAGCAGAAGAACGGCATCAAGGTG AACTTCAAGATCCGCCACAACATCGAGGACGGCAGCGTGCAGCTCG CCGACCACTACCAGCAGAACACCCCCATCGGCGACGGCCCCGTGCT GCTGCCCGACAACCACTACCTGAGCACCCAGTCCAAGCTGAGCAAA GACCCCAACGAGAAGCGCGATCACATGGTCCTGCTGGAGTTCGTGA CCGCCGCCGGGATCACTCTCGGCATGGACGAGCTGTACAAGtctagaG GGCAACCCGGGAACGGCAGCGCCTTCTTGCTGGCACCCAATAGAAG CCATGCGCCGGACCACGACGTCACGCAGCAAAGGGACGAGGTGTG GGTGGTGGGCATGGGCATCGTCATGTCTCTCATCGTCCTGGCCATC GTGTTTGGCAATGTGCTGGTCATCACAGCCATTGCCAAGTTCGAGCG TCTGCAGACGGTCACCAACTACTTCATCACTTCACTGGCCTGTGCTG AATTC	Donor sequence (1.2 kbp) encoding for mEGFP plus 230bp homology arms flanked by HindIII (5') and EcoRI (3') restriction enzyme sites which were used for cloning into a pcDNA3.1(+) vector backbone. Served as template to generate the hybrid dsDNA HDR donor cocktail for knock-in of mEGFP at the *ADRB2* locus.
crRNA-69forw	CTGCGCGCCATGGTGAGCAA	crRNA used in combination with generic tracrRNA to build the gRNA for Cas9 targeting to *mEGFP-ADRB2* locus. Binds over start codon for knock-in of HA signal sequence
ssODN for knock-in of HA	TGGGTCCGCCCGCTGAGGCGCCCCCAG CCAGTGCGCTCACCTGCCAGACTGCGC GCCATGAAGACGATCATCGCCCTGAGCT ACATCTTCTGCCTGGTATTCGCCGTGAG CAAGGGCGAGGAGCTGTTCACCGGGGT GGTGCCCATCCTGGTCGAGCTGGACGG C	ssODN consisting of 60 bp homology arms used as HDR donor template for knock-in of HA signal sequence at the N-terminus of *mEGFP-ADRB2* locus.
mEGFP_N-term_f	ATGGTGAGCAAGGGCGAGGA	Forward primer for generation of hybrid dsDNA HDR donor cocktail, binds N-terminus of *mEGFP*

mEGFP_C-term_linker_r	tctagaCTTGTACAGCTCGTCC	Reverse primer for generation of hybrid dsDNA HDR donor cocktail, binds C-terminus of *mEGFP* including a linker sequence
b2AR-hum_120bp_5'arm_f1	CCCACACCACAGCCGCTGAA	Forward primer for generation of hybrid dsDNA HDR donor cocktail, binds to 5'UTR of *ADRB2*
b2AR-hum_120bp_3'arm_r1	AGACATGACGATGCCCATGC	Reverse primer for generation of hybrid dsDNA HDR donor cocktail, binds to beginning of CDS of *ADRB2*
b2AR-hum_mEGFP-ADRB2_f1	ATTGGCCGAAAGTTCCCGTA	Forward sequencing primer: verification of endogenous insertion of HDR donor template at *ADRB2* locus, binds to end of 5'UTR of *ADRB2* and upstream of 5'-homology arm of HDR donor
b2AR-hum_mEGFP-ADRB2_r1	GTCCAAAACTCGCACCAGAA	Reverse sequencing primer: verification of endogenous insertion of HDR donor template at *ADRB2* locus, binds to beginning of CDS of *ADRB2* and downstream of 3'homology arm of HDR donor
2nd qPCR_GFP_Fwd	TGAGCAAAGACCCCAACGAG	Forward qPCR primer for amplification of *mEGFP-ADRB2*. Binds to C-terminus of *mEGFP*
2nd qPCR_ADRB2_Rev	CGCATGGCTTCTATTGGGTG	Reverse qPCR primer for amplification of mEGFP-ADRB2. Binds to N-terminus of *ADRB2*

CRISPR strategy

Efficient endogenous mEGFP-tagging at the N-terminus of *ADRB2* in hiPSC was achieved using CRISPR/Cas9 and hybrid asymmetric dsDNA-based donor cocktails as previously described [23]. A sequence-verified HDR donor plasmid was designed and purchased (Genscript) including the mEGFP sequence as well as 230 bp homology arms (refer to "Oligonucleotides"). Two different primer pairs were used to generate two PCR products from this donor plasmid encoding for: mEGFP alone and mEGFP plus 120bp 5' as well as 3' homology arms (refer to "Oligonucleotides"). A subsequent melt and anneal reaction led to generation of partially single-stranded "hybrid" donor with symmetric homology arms. This donor cocktail was provided to the cells together with a ribonucleoprotein complex consisting of crRNA, tracrRNA and Cas9 protein (Refer to "Oligonucleotides") via nucleofection using a 4D nucleofector (Lonza). Next, we generated single cell clones using automated hPSC single cell seeding and clonal expansion using the iotaSciences IsoCell platform [24]. We screened for GFP knockin at ARDB2 locus by PCR and selected one homozygous and one heterozygous clone for

further experiments. Single cell clones were generated and homozygous (clone #16) and heterozygous (clone #66) hiPSC clones were identified via PCR on genomic DNA.

A 2nd CRISPR round was performed on these two mEGFP-*ADRB2* CRISPRed clones #16 and #66 in order to introduce the HA signal sequence at the N-terminus of *mEGFP-ADRB2*. For this, a ssODN including the HA-signal sequence as well as 60bp homology arms was designed and purchased (IDT) and provided to the cells together with a novel crRNA as described above. Single cell clones were generated and homozygous (16-31) and heterozygous (66-35) hiPSC clones were identified via PCR on genomic DNA.

Contractility

Cells were imaged in 6-well dishes in brightfield mode on a custom build Zeiss setup. Time series videos of 3-5 min length were acquired before treatment, after antagonist incubation (100 nM ICI-118551, 300 nM CGP-20712A, 10 µM propranolol) and within 30 min after agonist treatment (1 µM isoproterenol). Contraction rates and other parameters were extracted from videos using the imageJ software “Myocyter v1.3” [25].

qRT-PCR

Cells were lysed and RNA extracted according to the RNeasy Mini kit (Qiagen). The cDNA synthesis was performed using the SuperScript III First-Strand Synthesis SuperMix (Invitrogen). Finally, qRT-PCR was done using the QuantiTect SYBR Green PCR kit (Qiagen) on an QuantStudio 6 flex qPCR device (ThermoFisher). Primers for GAPDH (Geneglobe ID: QT00079247) and *ADRB2* (Geneglobe ID: QT00200011) were purchased from Qiagen and primers for mEGFP-ADRB2 were self-made (refer to “Oligonucleotides”).

IF-staining

Cells were seeded in 8-well ibidi plates and washed with 250 µl PBS per well at the day of fixation. Cells were fixed using 4% paraformaldehyde for 30 min at room temperature (RT). Afterwards cells were washed again with PBS and stored at 4°C. Cells were blocked using NDS buffer (10% NDS, 0.2% BSA, 0.3% TritonX100) for 1 hour at RT and directly labelled overnight at 4°C with primary antibodies (1:400 mouse mAB for sarcomeric alpha-actinin [CloneEA-53, Sigma-Aldrich, A7811] and 1:200 rabbit pAB for cardiac Troponin T [Abcam, ab45932]). After washing cells once with PBS, secondary antibodies were applied for 2h in the dark (1:250 anti rabbit IgG coupled to AlexaFluor-555 [A31572] and 1:250 anti mouse IgG coupled to AlexaFluor-488 [A21202]). Two drops of NucBlue™ Fixed Cell ReadyProbes™ (Invitrogen, R37606) were added to the secondary Ab solution to also stain for nuclei. Cells were washed twice with PBS and then imaged on a Leica SP8 WLL.

Acquisition of line scans

In order to extract the behavior of the diffusing species linescan-FCS (Fluorescence Correlation Spectroscopy) was performed in which a confocal beam is repeatedly scanned at high speed over the same portion of the sample. The resultant recorded

kymographs or linescans are further analyzed by a custom-implemented code in MATLAB to extract information about diffusion data of receptors from autocorrelation functions (as previously described in (5)).

In short, linescans were acquired on a commercial confocal laser scanning microscope, Leica SP8 WLL, with a white light laser (WLL). Via the HC PLAP CS2 40x1.3 NA oil immersion objective (Leica) a pixel size of 50 nm was used to acquire about 6 x 105 lines of 256 pixels each at a speed of 1800 Hz. In order to stabilize the focal position, the IR laser based autofocus of the microscope (Leica, Adaptive Focus Control) was enabled while the ligand was excited at a wavelength of 633 nm with 5% laser power which upon calibration corresponded to approximately 3 µW. Hybrid detectors (HyD) in photon counting mode were applied to detect emission in the ranges of 460-540 nm (CFP) or 650-751 nm (Alexafluor 647-based JE1319). The beam waist was extracted by observation of the profiles of fluorescent microspheres (Tetraspeck, Thermofisher Scientific) as in (6) resulting in a lateral waist of $\omega_0^{(633\ nm)}$= 0.33 µm. A sample incubator (Stage Top Chamber, OKOlab) mounted on the stage of the Leica SP8 was used to keep cells at physiological conditions (37°C, 5% CO2) during imaging.

Analysis of confocal linescans

Confocal linescans were analyzed as previously described [12, 14]. Briefly, fluorescence correlation spectroscopy (FCS) extracts information on equilibrium processes in the sample by comparing statistical fluctuations of fluorescent particles in an effective detection volume. Linescan FCS greatly increases the statistical accuracy of these measurements due to the repeated scanning of one line. The recorded time-trace of fluorescent intensity (I) fluctuations in the effective detection volume allows for the calculation of an autocorrelation G(τ) reflecting the time-scale of these fluctuations.

$$G(\tau) = \frac{\langle I(t) \cdot I(t+\tau) \rangle}{\langle I(t) \rangle^2}$$

The pointed brackets represent the average over all time values t. In order to extract diffusion parameters, such as the diffusion time τ_D or the diffusion constant D (which are connected via $\tau_D = \frac{\omega_0^2}{4D}$), the autocorrelation function G(τ) is fit to the two-dimensional model of the autocorrelation function.

$$G_{2D}(\tau) = \frac{1}{N} \frac{1}{1 + \frac{4D\tau}{\omega_0^2}} + G_\infty$$

Where τ represents the time lag, N the average number of particles and G_∞ the limiting value of G(τ) for $\tau \to \infty$. ω_0 is the beam waist, and describes the extent of the effective detection volume in the focal plane where the intensity has dropped to e^{-2}.

In particular, an initial removal of the first 180225 lines of each scan reduces the influence of photo bleaching. The analysis is further corrected for bleaching via a moving average. A high pass filter reduces slow fluctuations by dividing the total time into smaller pieces of about 36:25 s.

The autocorrelation curves are normalized to the curve's G(0). In the case that no correlation was extracted the curves are normalized to its highest peak.

Acknowledgments

We would like here to acknowledge Dr. Peter Gmeiner for kindly sharing the JE1319 ligand. We shall further acknowledge excellent technical support from Marlies Grieben, Bärbel Pohl and Atakan Aydin. We acknowledge the MDC technology platform Pluripotent Stem Cells for technical support. This project was funded by the Deutsche Forschungsgemeinschaft (DFG, German Research Foundation) through Project 421152132 SFB1423 subproject C03 (PA, MJL) and SFB 1470 subproject A01 (PA).

Author contributions

P.G. and P.A. conceived the study and designed research. P.G. performed research with support from N.T. on generation of CRISPR clones and stem cell handling/differentiation. P.G. analyzed data. M.B.-P. analysed linescan FCS data and provided the software for this. P.G. and M.B.-P. prepared the figures. P.A. drafted the manuscript with contributions from P.G. and M.B.-P. The manuscript was edited by P.G., M.B-P. and N.T. All authors reviewed and approved the final manuscript. P.A. initiated and supervised the research. P.A. and M.J.L acquired funding.

Supplementary Figures

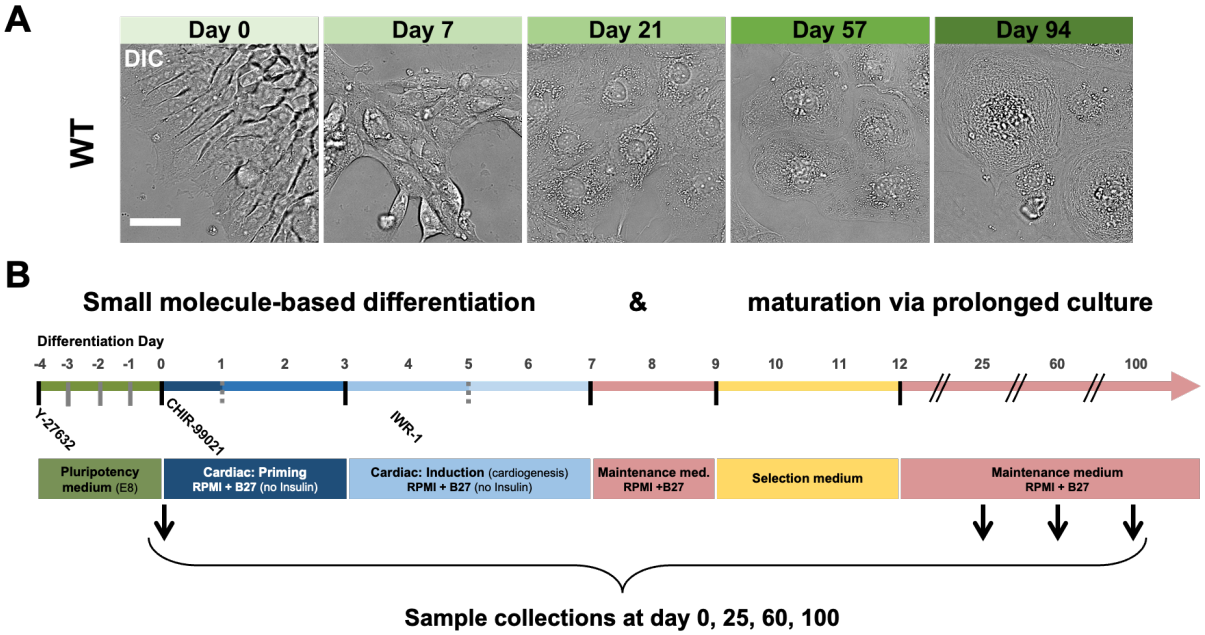

Supplemental Figure 1 Timeline displaying differentiation and maturation of hiPSC-CMs. (A) Shows changes of cellular morphology of undifferentiated WT hiPSC (day 0) and WT cells differentiated and matured for 7, 21, 57 and 94 days in culture. (B) Differentiation strategy based on small molecules depicting the most important treatment media indicated by day and duration of treatment and days of sample collection (25 +/-4 days; 60 +/-4 days; 100 +/-7 days).

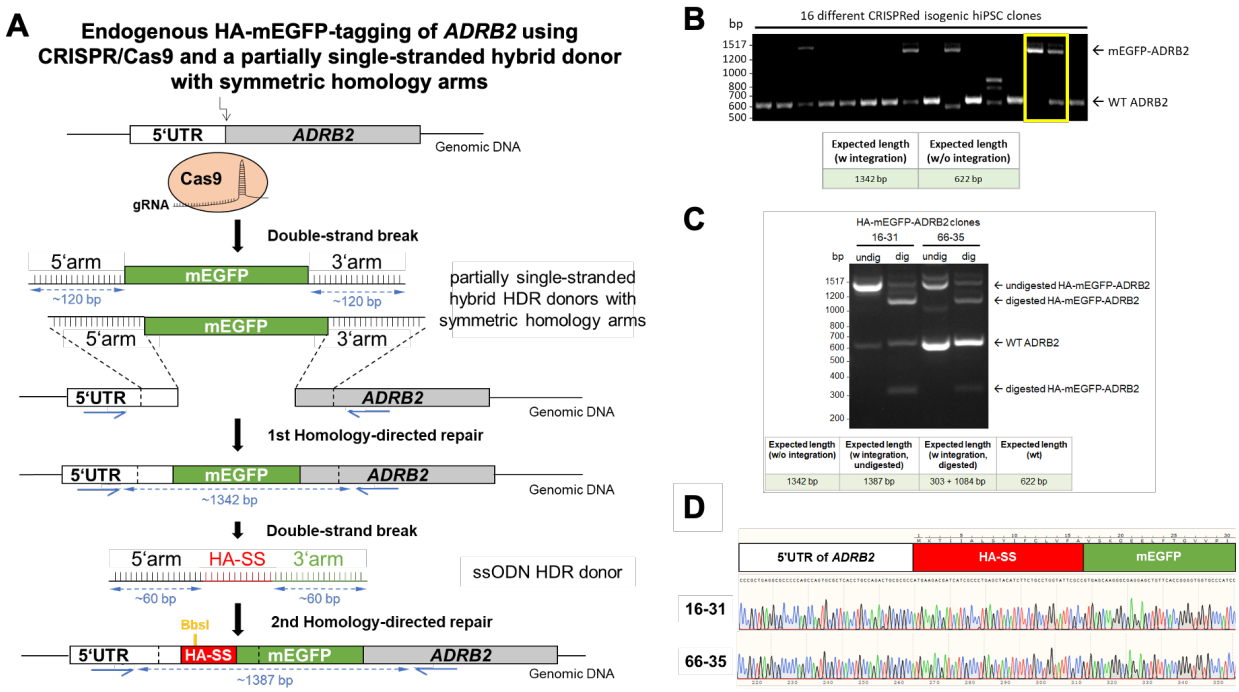

Supplemental Figure 2 Strategy for generation of the endogenously CRISPRed *mEGFP-ADRB2* clones. (A) Schematic of the 2-step CRISPR approach for N-terminal mEGFP-tagging of *ADRB2* based on an asymmetric-hybrid dsDNA-based HDR donor cocktail for the 1st homology directed repair. In a 2nd CRISPR round the membrane targeting Hemagglutinin signal sequence (HA-SS) was introduced endogenously at the N-terminus of *mEGFP-ADRB2* using a ssODN HDR donor [26]. (B) Genotyping of 16 CRISPRed isogenic hiPSC clones on agarose gel after 1st homology-directed repair based on genomic PCR using primers that bind outside the homology arms of the HDR donor as indicated in (A). Representative homozygous (clone 16) and heterozygous (clone 66) clones are highlighted in yellow. (C) Genotyping of several isogenic *HA-mEGFP-ADRB2* CRISPRed clones which were derived from clone 16 and clone 66 (highlighted in (B)) after using them for the 2nd CRISPR round (introducing HA-SS). (D) Shows DNA chromatograms of clones 16-31 and 66-35 based on Sanger sequencing at their CRISPRed *ADRB2* loci verifying correct in frame integration of the HA-mEGFP sequence at the N-terminus of *ADRB2*.

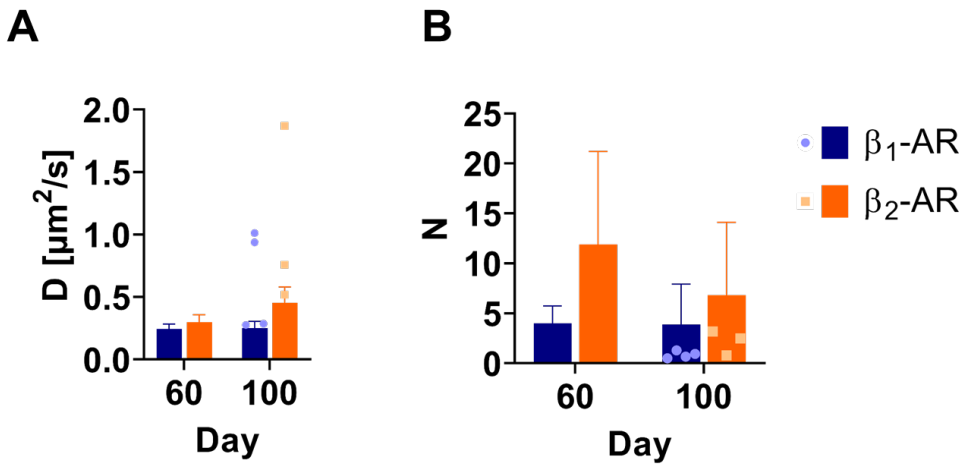

Supplemental Figure 3 (A) Mean diffusion constants and (B) mean number of particles extracted from the autocorrelation curves in Figure 3. Error bars represent SD values. Dots and small squares indicate diffusion constants and receptor numbers extracted at day 107 (and are not part of the day 100 mean).

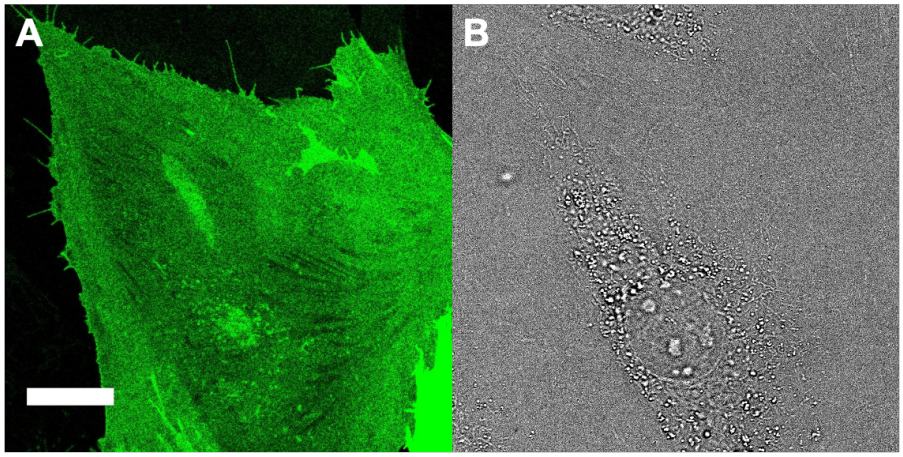

Supplemental Figure 4 *HA-mEGFP-ADRB2* overexpression in H9c2 cells. (A) Confocal micrograph of the basolateral membrane of an H9c2 cell expressing the construct HA-mEGFP-*ADRB2*, excited at 488 nm. (B) corresponding DIC image. Scale bar is 20 μm.

References

1. Guo, Y. and W.T. Pu, *Cardiomyocyte Maturation: New Phase in Development.* Circ Res, 2020. **126**(8): p. 1086-1106.
2. Babiarz, J.E., et al., *Determination of the human cardiomyocyte mRNA and miRNA differentiation network by fine-scale profiling.* Stem Cells Dev, 2012. **21**(11): p. 1956-65.
3. Grancharova, T., et al., *A comprehensive analysis of gene expression changes in a high replicate and open-source dataset of differentiating hiPSC-derived cardiomyocytes.* Sci Rep, 2021. **11**(1): p. 15845.
4. Liu, Q., et al., *Genome-Wide Temporal Profiling of Transcriptome and Open Chromatin of Early Cardiomyocyte Differentiation Derived From hiPSCs and hESCs.* Circ Res, 2017. **121**(4): p. 376-391.
5. Wu, H., et al., *Epigenetic Regulation of Phosphodiesterases 2A and 3A Underlies Compromised beta-Adrenergic Signaling in an iPSC Model of Dilated Cardiomyopathy.* Cell Stem Cell, 2015. **17**(1): p. 89-100.
6. Brodde, O.E., *Beta 1- and beta 2-adrenoceptors in the human heart: properties, function, and alterations in chronic heart failure.* Pharmacol Rev, 1991. **43**(2): p. 203-42.
7. Engelhardt, S., et al., *Progressive hypertrophy and heart failure in beta1-adrenergic receptor transgenic mice.* Proc Natl Acad Sci U S A, 1999. **96**(12): p. 7059-64.
8. Jung, G., et al., *Time-dependent evolution of functional vs. remodeling signaling in induced pluripotent stem cell-derived cardiomyocytes and induced maturation with biomechanical stimulation.* FASEB J, 2016. **30**(4): p. 1464-79.
9. Hasan, A., et al., *Age-Dependent Maturation of iPSC-CMs Leads to the Enhanced Compartmentation of beta2AR-cAMP Signalling.* Cells, 2020. **9**(10).
10. Kondrashov, A., et al., *Simplified Footprint-Free Cas9/CRISPR Editing of Cardiac-Associated Genes in Human Pluripotent Stem Cells.* Stem Cells Dev, 2018. **27**(6): p. 391-404.
11. Yan, L., et al., *Beta-adrenergic signals regulate cardiac differentiation of mouse embryonic stem cells via mitogen-activated protein kinase pathways.* Dev Growth Differ, 2011. **53**(6): p. 772-9.
12. Bathe-Peters, M., et al., *Visualization of beta-adrenergic receptor dynamics and differential localization in cardiomyocytes.* Proc Natl Acad Sci U S A, 2021. **118**(23).
13. Nikolaev, V.O., et al., *Beta2-adrenergic receptor redistribution in heart failure changes cAMP compartmentation.* Science, 2010. **327**(5973): p. 1653-7.
14. Bathe-Peters, M., et al., *Linescan microscopy data to extract diffusion coefficient of a fluorescent species using a commercial confocal microscope.* Data Brief, 2020. **29**: p. 105063.
15. Qian, T., et al., *Label-free imaging for quality control of cardiomyocyte differentiation.* Nat Commun, 2021. **12**(1): p. 4580.
16. Chorvat, D., Jr., et al., *Spectral unmixing of flavin autofluorescence components in cardiac myocytes.* Biophys J, 2005. **89**(6): p. L55-7.
17. Goulding, J., et al., *The use of fluorescence correlation spectroscopy to monitor cell surface beta2-adrenoceptors at low expression levels in human embryonic stem cell-derived cardiomyocytes and fibroblasts.* FASEB J, 2021. **35**(4): p. e21398.
18. Soave, M., et al., *Detection of genome-edited and endogenously expressed G protein-coupled receptors.* FEBS J, 2021. **288**(8): p. 2585-2601.
19. Liu, Y., A. Beyer, and R. Aebersold, *On the Dependency of Cellular Protein Levels on mRNA Abundance.* Cell, 2016. **165**(3): p. 535-50.

20. Tahmasebi, S., M. Amiri, and N. Sonenberg, *Translational Control in Stem Cells.* Front Genet, 2018. **9**: p. 709.
21. Patwardhan, A., N. Cheng, and J. Trejo, *Post-Translational Modifications of G Protein-Coupled Receptors Control Cellular Signaling Dynamics in Space and Time.* Pharmacol Rev, 2021. **73**(1): p. 120-151.
22. Lian, X., et al., *Robust cardiomyocyte differentiation from human pluripotent stem cells via temporal modulation of canonical Wnt signaling.* Proc Natl Acad Sci U S A, 2012. **109**(27): p. E1848-57.
23. Dokshin, G.A., et al., *Robust Genome Editing with Short Single-Stranded and Long, Partially Single-Stranded DNA Donors in Caenorhabditis elegans.* Genetics, 2018. **210**(3): p. 781-787.
24. Vallone, V.F., et al., *Methods for Automated Single Cell Isolation and Sub-Cloning of Human Pluripotent Stem Cells.* Curr Protoc Stem Cell Biol, 2020. **55**(1): p. e123.
25. Grune, T., et al., *The "MYOCYTER" - Convert cellular and cardiac contractions into numbers with ImageJ.* Sci Rep, 2019. **9**(1): p. 15112.
26. Isbilir, A., et al., *Determination of G-protein-coupled receptor oligomerization by molecular brightness analyses in single cells.* Nat Protoc, 2021. **16**(3): p. 1419-1451.